Energy consumption investigation for a new car-following model considering driver's memory and average speed of the vehicles

Zhizhan-Jin[1,2,3], Zaili-Yang[4], Rongjun-Cheng[1,2,3], Hongxia-Ge[1,2,3]

[1)] *Faculty of Maritime and Transportation, Ningbo University, Ningbo 315211, China;*

[2)] *Jiangsu Province Collaborative Innovation Center for Modern Urban Traffic Technologies, Nanjing 210096, China;*

[3)] *National Traffic Management Engineering and Technology Research Centre Ningbo University Sub-centre, Ningbo 315211, China;*

[4)]

In this paper, a modified car-following model is proposed by taking into account the influence of the average speed effect of the vehicles and driver's memory on traffic flow basing on the two velocity difference model (TVDM). The stability conditions are obtained through the linear stability analysis. The time-dependent Ginzburg-Landau (TDGL) equation and the modified Korteweg-de Vries (mKdV) equation are derived in the unstable area by means of nonlinear analysis, respectively. The TDGL and mKdV equations are constructed to describe the traffic behavior near the critical point. The evolution of traffic congestion and the corresponding energy consumption are discussed. Numerical simulations are in good agreement with the theoretical results. It is found that the extended model can not only to depress the energy consumption but also to enhance the stability of traffic flow.

Keywords: Traffic flow; Driver's memory; Average speed; Energy consumption; T-DGL equation

1. Introduction

In recent years, the traffic problem did more and more influence on the development of the city and the rhythm of human life. In order to solve this problem, a large number of traffic models have been proposed to research the complex traffic phenomena. Such as the substantial traffic models [1-10] which mainly include car-following models [11-19], cellular automation models [20-23], gas kinetic models [24-26], and hydrodynamic lattice models [27-29] have been posed to study traffic flow. The optimal velocity model (for short OVM) was firstly proposed by Bando et al. [30] in 1995, which has successfully revealed the dynamic evolution of traffic

jam in a simple way. The equation of motion is shown as follows:

$$\frac{dv_n(t)}{dt} = a[V(\Delta x_n(t)) - v_n(t)] \tag{1}$$

where $v_n(t)$ is the velocity of car n at time t, $\Delta x_n(t) = x_{n+1}(t) - x_n(t)$ represents the headway of two successive vehicles, a is the sensitivity coefficient of a driver, and $V(\Delta x_n(t))$ is the optimal velocity function.

However, the OVM has shortcomings of high acceleration rate and unrealistic deceleration. To solve the drawbacks of OVM, Helbing and Tilch [31] put forward a generalized force model (for short GFM), i.e.

$$\frac{dv_n(t)}{dt} = a[V(\Delta x_n(t)) - v_n(t)] + \lambda H(-\Delta v_n(t))\Delta v_n(t) \tag{2}$$

where H is the Heaviside function, λ is a sensitivity coefficient different from a, $\Delta v_n(t) = v_{n+1}(t) - v_n(t)$ is the velocity difference between the leading car $n+1$ and the following car n. Jiang et al.[32,33] developed the full velocity difference model (FVDM). The study shows that the FVDM is in agreement with the field data better than OVM and GFM.

$$\frac{dv_n(t)}{dt} = a[V(\Delta x_n(t)) - v_n(t)] + \lambda \Delta v_n(t) \tag{3}$$

However, the deceleration of FVDM is too high. In order to solve the deficiency, Ge et al.[34] proposed the two velocity difference model (for short, TVDM) by considering the ITS application.

$$\frac{dv_n(t)}{dt} = a[V(\Delta x_n(t)) - v_n(t)] + \lambda\,[p\Delta v_n(t) + (1-p)\Delta v_{n+1}(t)] \tag{4}$$

Comparing with the above models, TVDM and FVDM have better agreement with the field data than OVM and GFM.

In recent years, with the improvement of the quality of people's living standards, traffic problems are becoming more and more serious in modern city. In particular, the problem of energy consumption caused by traffic congestion has become a hot issue, and it has attracted the attention of many scholars. The real traffic is affected by many complicated factors such as capability, average speed, drivers' sensitivity and so on. These main factors on the uniform traffic flow are treated as disturbance to lead to the change of the vehicle velocity, which spreads like a wave. Therefore, this change of velocity will result in the added energy consumption.

In addition, we consider the relationship between energy consumption and vehicle stability. On the basis of the kinetic energy theorem, the energy consumption of each vehicle on a road can be researched in more details, which describes every vehicle to do work by consuming energy. Through describing the change of the vehicle in two adjacent moments, the change of the kinetic energy is defined as:

$$\Delta E_i = \frac{1}{2}[v_i^2(t) - v_i^2(t-1)] \tag{5}$$

where $v_i(t)$ and $v_i(t-1)$ are the velocity of vehicle i in the two successive time steps.

Basing on the above analysis, these models can explain some complex and real traffic phenomena. Besides, the following car driver always need a period of time to respond for current traffic conditions in real traffic environment. Therefore, we should try to shorten the time as much as possible. In fact, the average speed of the vehicle group front reflects the whole traffic condition. However, these models are not suitable for the study of the average speed effect of the vehicle group because the predecessors did not think about this factor. Therefore, a extended car-following model is presented based on the TVDM taking into account the influence of the average speed [35,36] effect of the vehicles and the driver's memory [37,38] on traffic flow. This is the main difference with other models.

In Sect. 2, the improved model is presented with considering the driver's memory and jerk based on TVDM. The stable condition is analyzed by using linear stability theory. In Sect. 3, the new model is analyzed by the nonlinear analysis near the critical point, and the TDGL equation is obtained. In Sect. 4, the mKdV equation is derived. In Sect. 5, numerical simulation is given. In Sect. 6, the conclusions are drawn.

2. The improved model and linear stability analysis

Basing on TVDM, we proposed an improved car-following model considering the influence of the average speed effect of the vehicles and driver's memory on traffic flow. The main motion equation is shown as follows:

$$\begin{aligned}\frac{dv_n(t)}{dt} = a[V(\frac{1}{\tau_0}\int_{t-\tau_0}^{t}\Delta x_n(u)du) - v_n(t)] + +\lambda_1[\frac{1}{n}\sum_{l=1}^{n}\frac{dx_{n+l}(t)}{dt} - \frac{dx_n(t)}{dt}] \\ +\lambda_2[p\Delta v_n(t) + (1-p)\Delta v_{n+1}(t)]\end{aligned} \tag{6}$$

where $\frac{1}{n}\sum_{l=1}^{n}\frac{dx_{n+l}(t)}{dt}$ is the average speed term between the car n and its leading cars n, $n+1$, $n+2$, ..., $n+n$ at time t. $\Delta x_n(u) = x_{n+1}(u) - x_n(u)$ is the headway between the preceding car $n+1$ and the following car n, a is the sensitivity which corresponds to the inverse of the delay time, τ_0 is driver's memory time, λ_1 is the responding factor to the difference between the average speed and velocity and λ_2 is the two velocity difference model parameter. The optimal velocity function is proposed [30].

$$V(\Delta x_n(t)) = \frac{v_{max}}{2}[\tanh(\Delta x_n(t) - h_c) + \tanh(h_c)] \tag{7}$$

where v_{max} is the maximal velocity and h_c is the safety distance. The function $V(.)$ is a monotonically increasing function with an upper bound (maximal velocity) and has a turning point $\Delta x_n = h_c : V''(h_c) = 0$. For convenience of linear analysis, Eq.(6) can be rewritten as:

$$\begin{aligned}\frac{d^2x_n(t)}{dt^2} = a[V(\frac{1}{\tau_0}\int_{t-\tau_0}^{t}\Delta x_n(u)du) - \frac{dx_n(t)}{dt}] + \lambda_1[\frac{1}{n}\sum_{l=1}^{n}\frac{dx_{n+l}(t)}{dt} - \frac{dx_n(t)}{dt}]+ \\ \lambda_2[p(\frac{dx_{n+1}(t)}{dt} - \frac{dx_n(t)}{dt}) + (1-p)(\frac{dx_{n+2}(t)}{dt} - \frac{dx_{n+1}(t)}{dt})]\end{aligned} \tag{8}$$

Furthermore, Eq.(8) can be rewritten in terms of the headway:

$$\begin{aligned}\frac{d^2\Delta x_n(t)}{dt^2} = a[V(\frac{1}{\tau_0}\int_{t-\tau_0}^{t}\Delta x_{n+1}(u)du) - V(\frac{1}{\tau_0}\int_{t-\tau_0}^{t}\Delta x_n(u)d_u) - \frac{d\Delta x_n(t)}{dt}]+ \\ \lambda_1[\frac{1}{n}\sum_{l=1}^{n}\frac{d\Delta x_{n+l}(t)}{dt} - \frac{d\Delta x_n(t)}{dt}] + \lambda_2[p(\frac{d\Delta x_{n+1}(t)}{dt} - \frac{d\Delta x_n(t)}{dt})+ \\ (1-p)(\frac{d\Delta x_{n+2}(t)}{dt} - \frac{d\Delta x_{n+1}(t)}{dt})]\end{aligned} \tag{9}$$

It is obvious that the traffic flow can reach the steady state when the vehicle run with constant headway h and constant velocity $V(h)$. So, the steady-state solution is given as:

$$x_n^0(t) = hn + V(h)t, h = \frac{L}{N} \tag{10}$$

where N is the total vehicle number and L is the road length.

Suppose $y_n(t)$ is a small deviation from the steady state $x_n^0(t) : x_n(t) = x_n^0(t) + y_n(t)$. Substitute it into Eq.(8) and linearize it which yields

$$\begin{aligned}\frac{{dy_n}^2(t)}{dt^2} = a[V'(h)(\frac{1}{\tau_0}\int_{t-\tau_0}^{t}\Delta y_n(u)du) - \frac{dy_n(t)}{dt}] + \lambda_1[\frac{1}{n}\sum_{l=1}^{n}\frac{dy_{n+l}(t)}{dt} - \frac{dy_n(t)}{dt}] \\ \lambda_2[p(\frac{dy_{n+1}(t)}{dt} - \frac{dy_n(t)}{dt}) + (1-p)(\frac{dy_{n+2}(t)}{dt} - \frac{dy_{n+1}(t)}{dt})]\end{aligned} \tag{11}$$

where $\Delta y_n(t) = y_{n+1}(t) - y_n(t)$ and $V'(h) = dV(\Delta x_n)dt|\Delta x_n = h$. Expanding $y_n(t) = exp(ikn + zt)$, it reads

$$z^2 = a[V'(e^{ik} - 1)e^{-z\gamma\tau_0} - z] + \lambda_1 z(\frac{1}{n}\sum_{l=1}^{n} e^{ikl} - 1) + \lambda_2 z[p(e^{ik} - 1) + (1-p)(e^{2ik} - e^{ik})] \quad (12)$$

where $V' = V'(h)$. Let $z = z_1(ik) + z_2(ik)^2 + \cdots$, then the first-and second-order terms of ik are:

$$z_1 = V'(h), z_2 = \frac{V'}{2} - \gamma\tau_0 V'^2 + \frac{\lambda_1 V'}{na}\sum_{l=1}^{n} l + \frac{\lambda_2 V' - V'^2}{a} \quad (13)$$

Denote $\tau_0 = s\tau$, $s > 0$ is the proportionality coefficient of τ_0 with τ. The parameter γ represents the driver' s memory intensity. For small disturbance with long wavelengths, the uniform traffic flow is instable in the condition that

$$a < 2(1 + \gamma s)V' - 2(\lambda_2 + \frac{\lambda_1}{n}\sum_{l=1}^{n} l) \quad (14)$$

The stability condition is given:

$$a = 2(1 + \gamma s)V' - 2\lambda_2 - \lambda_1(1 + n) \quad (15)$$

Figure 1 shows the phase diagram in the (h, a)-plane where h is the headway and a is sensitivity which corresponds to the inverse of the delay time. The solid lines denote the results of the neutral stability curves with different the values of n and λ_2. It shows the stable region and unstable region from Fig.1, the critical points decrease with increasing the value of the parameter n.

From the pattern (a), (b) and (c) of Fig.1, we increase n (n=1, 4, 7) with the same λ_2, the stable region gradually increase and the the unstable region decrease piecemeal. As we can see from the pattern (a), (b) and (c) of Fig.1, the unstable region gradually increase when we take the same λ_2, with the decrease of n (n=7, 4, 1). As increasing λ_2, the stable region is increasing gradually with other parameters are unchanged from the pattern(d) of Fig.1. The traffic flow is more stable.

The result is relevant with the parameter n. ($v_{max} = 2, h_c = 4$)

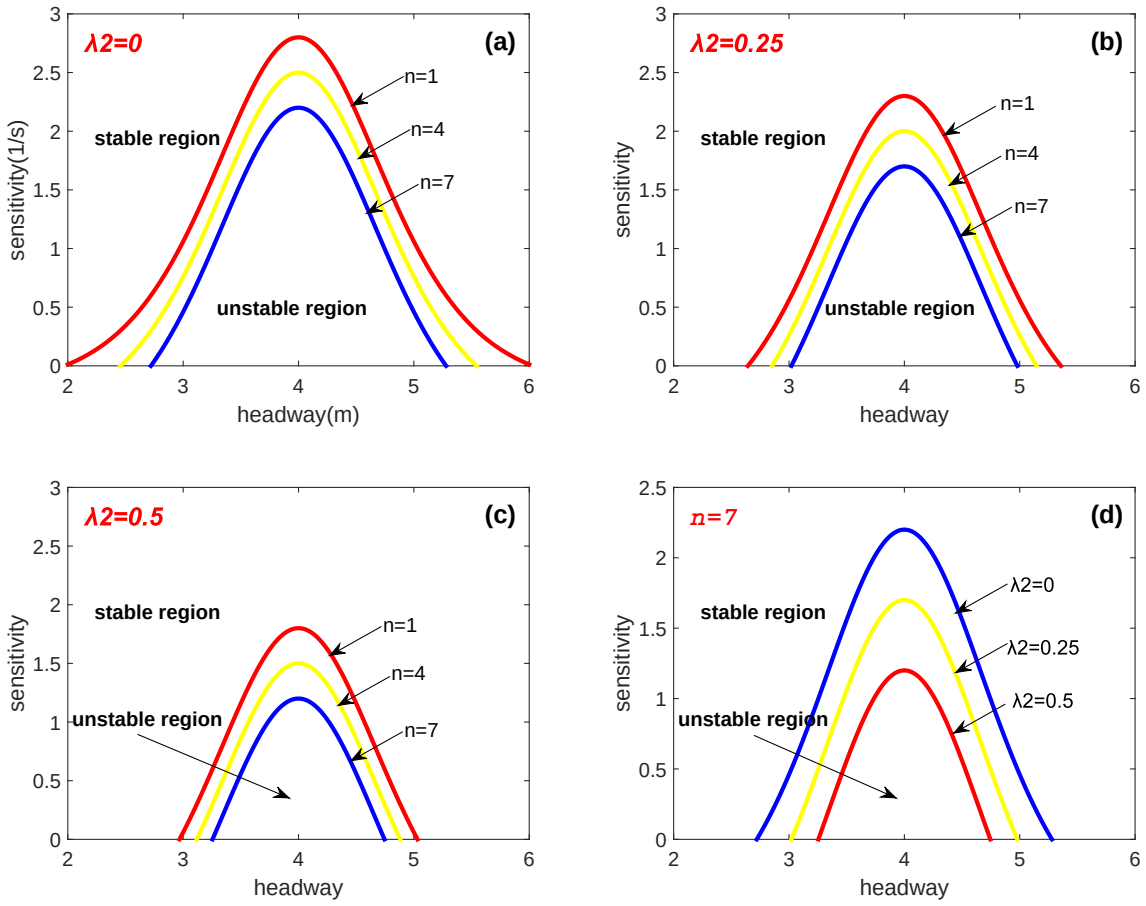

Fig.1. The phase diagram of the model according to different values of parameter n and λ_2

3. TDGL equation

In the car-following models, the nonlinear density wave equation is inferred to describe the propagation characteristics of traffic congestion. In this part, we employ the method of nonlinear analysis to research the traffic problems. On the coarse grain size, we describe the traffic flow by using the long wavelength models and then obtaining the solution of the equation. The slow change behavior of long waves near the critical point is analyzed. The slow scales for space variable j, time variable t and undetermined constant b are introduced, and the slow variables X and T are defined as follows:

$$X = \varepsilon(j + bt), T = \varepsilon^3 t, 0 < \varepsilon \ll 1. \tag{16}$$

The headway $\Delta x_n(t) = h_c + \varepsilon R(X, T)$ is set as:

$$\Delta x_n(t) = h_c + \varepsilon R(X, T). \tag{17}$$

By bringing Eqs.(16)-(17) into Eq.(9), and expanding to the fifth-order of ε. We get the expression:

$$\varepsilon^2(b-V')\partial_X R+\varepsilon^3[\tau b^2-\frac{1}{2}V'(1-2b\gamma\tau_0+2\lambda_2 b\tau)-\frac{\lambda_1 b\tau}{n}\sum_{l=1}^{n}l]\partial_X^2 R+$$
$$\varepsilon^4[\partial_T R+(\tau\lambda_1 b(p-\frac{3}{2})-\frac{1}{6}V'(1-3b\gamma\tau_0+3b^2\gamma^2\tau_0^2)-\frac{\lambda_1 b\tau}{2n}\sum_{l=1}^{n}l^2)\partial_X^3 R-\frac{V'''}{6}\partial_X R^3]$$
$$+\varepsilon^5[(2\tau b+\gamma\tau_0 V'-\lambda_2\tau-\frac{\lambda_1\tau}{n}\sum_{l=1}^{n}l)\partial_X\partial_T R+(\tau\lambda_1 b(p-\frac{7}{6})-\frac{\lambda_1 b\tau}{6n}\sum_{l=1}^{n}l^3-$$
$$\frac{1}{24}V'(1-4\gamma\tau_0 b+\frac{1}{6}\gamma^2\tau_0^2 b^2-4\gamma^3\tau_0^3 b^3))\partial_X^4 R-\frac{V'''}{12}(1-2\gamma\tau_0 b)\partial_X^2 R^3]=0 \tag{18}$$

Now, we consider the traffic flow near critical point $\tau=(1+\varepsilon^2)\tau_c$, $\tau_0=s\tau$, $s>0$. By taking $b=V'$, the second- and third-order terms of ε is eliminated from Eq.(18), which leads to the simplified equation as following

$$\varepsilon^4\partial_T R=\varepsilon^4[\frac{1}{6}V'(1-3V'\gamma\tau s+3V'^2\gamma^2\tau^2 s^2)-\lambda_2\tau V'(p-\frac{3}{2})+\frac{\lambda_1 V'\tau}{2n}\sum_{l=1}^{n}l^2]\partial_X^3 R-$$
$$\varepsilon^4\frac{|V'''|}{6}\partial_X R^3+\varepsilon^3\frac{V'}{2}[1-V'\gamma\tau s+2\lambda_2 V'\tau+(1+n)\lambda_1\tau-2V'\tau]\partial_X^2 R-$$
$$\varepsilon^5[(\lambda_2 V'\tau(p-\frac{3}{2})-\frac{\lambda_1 V'\tau}{2n}\sum_{l=1}^{n}l^2-\frac{V'}{6}(1-3V'\gamma\tau s+3V'^2\gamma^2\tau^2 s^2))(2V'\tau+V'\gamma\tau s-$$
$$\lambda_2\tau-\frac{\lambda_1\tau}{2}(1+n))+\lambda_2(p-\frac{7}{6})V'\tau-\frac{\lambda_1 V'\tau}{6n}\sum_{l=1}^{n}l^3-\frac{V'}{24}(1-4V'\gamma\tau s+$$
$$\frac{1}{6}V'^2\gamma^2\tau^2 s^2-4V'^3\gamma^3\tau^3 s^3)]\partial_X^4 R+\varepsilon^5\frac{|V'''|}{12}[1+4V'\tau-2\lambda_2\tau-\lambda_1\tau(1+n)]\partial_X^2 R^3 \tag{19}$$

By transforming variable X and T into variable $x=\varepsilon^{-1}X$ and $t=\varepsilon^{-3}T$, and taking $S(x,t)=\varepsilon R(X,T)$, Eq.(19) is rewritten as follows:

$$\partial_t S=[\frac{1}{6}V'(1-3V'\gamma\tau s+3V'^2\gamma^2\tau^2 s^2)-\lambda_2\tau V'(p-\frac{3}{2})+\frac{\lambda_1 V'\tau}{2n}\sum_{l=1}^{n}l^2]\partial_x^3 S-$$
$$\frac{|V'''|}{6}\partial_x S^3+\frac{V'}{2}[1-V'\gamma\tau s+2\lambda_2 V'\tau+(1+n)\lambda_1\tau-2V'\tau]\partial_x^2 S-$$
$$[(\lambda_2 V'\tau(p-\frac{3}{2})-\frac{\lambda_1 V'\tau}{2n}\sum_{l=1}^{n}l^2-\frac{V'}{6}(1-3V'\gamma\tau s+3V'^2\gamma^2\tau^2 s^2))(2V'\tau+V'\gamma\tau s-$$
$$\lambda_2\tau-\frac{\lambda_1\tau}{2}(1+n))+\lambda_2(p-\frac{7}{6})V'\tau-\frac{\lambda_1 V'\tau}{6n}\sum_{l=1}^{n}l^3-\frac{V'}{24}(1-4V'\gamma\tau s+$$
$$\frac{1}{6}V'^2\gamma^2\tau^2 s^2-4V'^3\gamma^3\tau^3 s^3)]\partial_x^4 S+\frac{|V'''|}{12}[1+4V'\tau-2\lambda_2\tau-\lambda_1\tau(1+n)]\partial_x^2 S^3 \tag{20}$$

By adding term $(V'+\gamma sV'-\lambda_2-\frac{1}{2}\lambda_1(1+n))[1-V'\gamma\tau s+2\lambda_2V'\tau+(1+n)\lambda_1\tau-2V'\tau]$ on both left and right sides of Eq.(20) and performing $t_1=t$ and $x_1=x-(V'+\gamma sV'-\lambda_2-\frac{1}{2}\lambda_1(1+n))[1-V'\gamma\tau s+2\lambda_2V'\tau+(1+n)\lambda_1\tau-2V'\tau]t$ for Eq.(20) we get

$$\partial_{t_1}S=(\partial_{x_1}-\frac{V'}{2(1+\gamma s)V'-2\lambda_2-\lambda_1(1+n)}\partial^2_{x_1})[(\frac{1}{6}V'(1-3V'\gamma\tau s+3V'^2\gamma^2\tau^2s^2)-$$
$$\lambda_2\tau V'(p-\frac{3}{2})+\frac{\lambda_1V'\tau}{2n}\sum_{l=1}^{n}l^2)\partial^2_{x_1}S-(V'+\gamma sV'-\lambda_2-\frac{1}{2}\lambda_1(1+n))$$
$$[1-V'\gamma\tau s+2\lambda_2V'\tau+(1+n)\lambda_1\tau-2V'\tau]S-\frac{V'''}{6}S^3] \tag{21}$$

We define the thermodynamic potentials:

$$\phi(S)\equiv-[\frac{1}{2}(1+\gamma s)V'-\frac{1}{2}\lambda_2-\frac{1}{4}\lambda_1(1+n)]$$
$$[V'\gamma\tau s-2\lambda_2V'\tau-(1+n)\lambda_1\tau+2V'\tau-1]S^2+\frac{|V'''|}{24}S^4 \tag{22}$$

By rewritten Eq.(21) with Eq.(22), the TDGL equation is derived

$$\partial_{t_1}S=-(\partial_{x_1}+\frac{V'}{2(1+\gamma s)V'-2\lambda_2-\lambda_1(1+n)}\partial^2_{x_1})\frac{\delta\Phi(S)}{\delta S} \tag{23}$$

$$\Phi(S)\equiv\int dx_1[(\frac{1}{6}V'(1-3V'\gamma\tau s+3V'^2\gamma^2\tau^2s^2)-$$
$$\lambda_2\tau V'(p-\frac{3}{2})+\frac{\lambda_1V'\tau}{2n}\sum_{l=1}^{n}l^2)(dx_1S)^2+\phi(S)] \tag{24}$$

where $\delta\Phi(S)/\delta S$ indicates the function derivative. The TDGL Eq.(23) has two steady-state solutions except trivial solution S=0: one is the uniform solution

$$S(x_1,t_1)=\pm[\frac{3(2(1+\gamma s)V'-2\lambda_2-\lambda_1(1+n))(2\lambda_2V'\tau-\lambda_1\tau+2V'\tau-1)}{|V'''|}]^{\frac{1}{2}} \tag{25}$$

And the other is the kink solution

$$S(x_1,t_1)=\pm[\frac{3(2(1+\gamma s)V'-2\lambda_2-\lambda_1(1+n))(2\lambda_2V'\tau-\lambda_1\tau+2V'\tau-1)}{|V'''|}]^{\frac{1}{2}}\times$$
$$tanh\left\{\left[\frac{(V'\gamma\tau s-2\lambda_2V'\tau+2V'\tau-1)(2(1+\gamma s)V'-2\lambda_2-\lambda_1(1+n))}{\frac{1}{24}V'(1-3V'\gamma\tau s+3V'^2\gamma^2\tau^2s^2)-\frac{1}{4}\lambda_2\tau V'+\frac{\lambda_1V'\tau}{8n}\sum_{l=1}^{n}l^2}\right]^{\frac{1}{2}}\times(x_1-x_0)\right\} \tag{26}$$

where x_0 is constant. Equation (26)represents the coexisting phase.By the condition

$$\partial\phi/\partial S=0,\partial^2\phi/\partial S^2>0 \tag{27}$$

We obtain the coexisting curve from Eq.(22) in terms of the original parameters

$$(\Delta x)_{co} = h_c \pm \pm[\frac{3(2(1+\gamma s)V' - 2\lambda_2 - \lambda_1(1+n))(2\lambda_2 V'\tau - \lambda_1\tau + 2V'\tau - 1)}{|V'''|}]^{\frac{1}{2}} \tag{28}$$

The spinodal line is given by the condition

$$\partial^2\phi/\partial S^2 = 0 \tag{29}$$

From Eq.(22), we obtain the spinodal line described by the following equation

$$(\Delta x)_{co} = h_c \pm \pm[\frac{(2(1+\gamma s)V' - 2\lambda_2 - \lambda_1(1+n))(2\lambda_2 V'\tau - \lambda_1\tau + 2V'\tau - 1)}{|V'''|}]^{\frac{1}{2}} \tag{30}$$

The critical point is given by the condition $\partial\phi/\partial S = 0$ and Eq.(29)

$$(\Delta x)_c = h_c, a_c = 2(1+\gamma s)V' - 2\lambda_2 - \lambda_1(1+n) \tag{31}$$

4. mKdV equation

Similarly, we discuss the slowly varying behavior at long wavelengths near the critical point with the derivation of the TDGL equation. We extract slow scale for space variable n and time variable t. By inserting $a_c = 2(1+\gamma s)V' - 2\lambda_2 - \lambda_1(1+n)$, $a = (1+\varepsilon^2)a_c$ into Eq.(18), one obtains:

$$\varepsilon^4(\partial_T R - j_1\partial_X^3 R + j_2\partial_X R^3) + \varepsilon^5(j_3\partial_X^2 R + j_4\partial_X^4 + j_5\partial_X^2 R^3) = 0 \tag{32}$$

Table 1: The coefficients j_i of the model

j_1	j_2	j_3
$\frac{V'}{6} + \frac{\frac{1}{2}V'^3\gamma^2 s^2}{[2(1+\gamma s)V' - 2\lambda_2 - \lambda_1(1+n)]^2} - \frac{\lambda_2(p-\frac{3}{2})V' - \frac{\lambda_1 V'}{2n}\sum_{l=1}^{n} l^2 + \frac{V'}{2}\gamma s}{2(1+\gamma s)V' - 2\lambda_2 - \lambda_1(1+n)}$	$-\frac{V'''}{6}$	$\frac{V'^2}{2(1+\gamma s)V' - 2\lambda_2 - \lambda_1(1+n)}$
j_4		
$\frac{\lambda_2(p-\frac{7}{6})V' - \frac{\lambda_1 V'}{6n}\sum_{l=1}^{n} l^2 + \frac{V'}{6}\gamma s}{2(1+\gamma s)V' - 2\lambda_2 - \lambda_1(1+n)} - \frac{\frac{1}{6}\gamma^2 s^2 V'^3}{24[2(1+\gamma s)V' - 2\lambda_2 - \lambda_1(1+n)]^2} + \frac{\gamma^3 s^3 V'^4}{6[2(1+\gamma s)V' - 2\lambda_2 - \lambda_1(1+n)]^3} - \frac{V'}{24}$		
j_5		
$\frac{V'''}{6}[\frac{(3V'+\gamma s)V' - 2\lambda_2 - \lambda_1(1+n)}{2(1+\gamma s)V' - 2\lambda_2 - \lambda_1(1+n)}]$		

where the coefficients j_i are given in Table 1.

In the table $V' = dV(\Delta x_n)/d\Delta x_n|\Delta x_n = h_c$, $V''' = d^3V(\Delta x_n)/d\Delta x_n^3|\Delta x_n = h_c$. In order to derive the regularized equation, we make the following transformation:

$$T = \frac{1}{j_1}T', R = \sqrt{\frac{j_1}{j_2}} \tag{33}$$

So the standard mKdV equation with an $O(\varepsilon)$ correction term as follows:

$$\partial_{T'}R' = \partial_X^3 R' - \partial_X R'^3 - \varepsilon[\frac{j_3}{j_1}\partial_X^2 R' + \frac{j_4}{j_1}\partial_X^4 R' + \frac{j_5}{j_2}\partial_X^2 R'^3] \tag{34}$$

If we ignore the $O(\varepsilon)$, they are just the mKdV equations with a kink solution as the desired solution:

$$R_o'(X, T') = \sqrt{c}tanh\sqrt{\frac{c}{2}}(X - cT') \tag{35}$$

Then, assuming that $R'(X, T') = {R_o}'(X, T') + \varepsilon {R_1}'(X, T')$, we take into account the $O(\varepsilon)$ correction. For the purpose of determining the selected value of the velocity c for the kink solution, it is necessary to satisfy the solvability condition. As $({R_o}', M[{R_o}']) \equiv \int_{-\infty}^{+\infty} dX' {R_o}' M[R']$, where $M[{R_o}'] = \frac{j_3}{j_1}\partial_X^2 R' + \frac{j_4}{j_1}\partial_X^4 R' + \frac{j_5}{j_2}\partial_X^2 R'^3$. We get the general velocity c:

$$c = \frac{5j_2j_3}{2j_2j_4 - 3j_1j_5} \tag{36}$$

Hence, the general kink-antikink soliton solution of the headway, from the mKdV equation is obtained:

$$\Delta x_n(t) = h_c \pm \sqrt{\frac{j_1 c}{j_2}(\frac{\tau}{\tau_c} - 1)} \times tanh\sqrt{\frac{c}{2}(\frac{\tau}{\tau_c} - 1)} \times [n + (1 - cj_1)(\frac{\tau}{\tau_c} - 1)t] \tag{37}$$

where $V''' < 0$, this kink soliton solution also represents the coexisting phase, and the kink solution(37) is agree with the solution(26) obtained from the TDGL equation. Thus, the jamming transition can be described by both the TDGL equation with a nontravelling solution and the mKdV equation with a propagating solution.

5. Numerical simulation

In this section, we carried out the numerical simulation by the computer. With the periodic boundary condition, the initial conditions are given as follows:

$\Delta x_j(0) = \Delta x_0 = 4.0, \Delta x_j(1) = \Delta x_0 = 4.0$, for $j \neq 50, 51$, $\Delta x_j(1) = 4.0 - 0.5$, for $j = 50, \Delta x_j(1) = 4.0 + 0.5$, for $j = 51$

We choose the total number of cars and the sensitivity as $N = 100$ and $a = 1.7$.

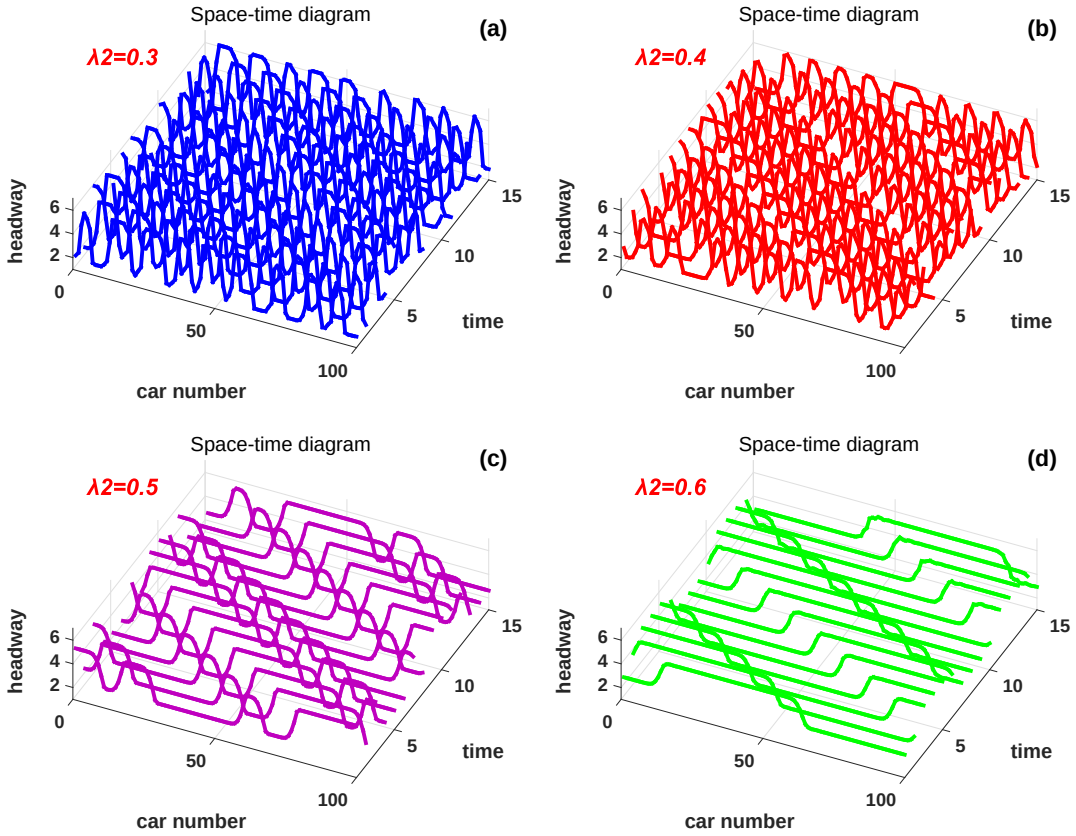

Fig.2 Space – time evolution of the headway after t=10,000 with the different λ_2-values.

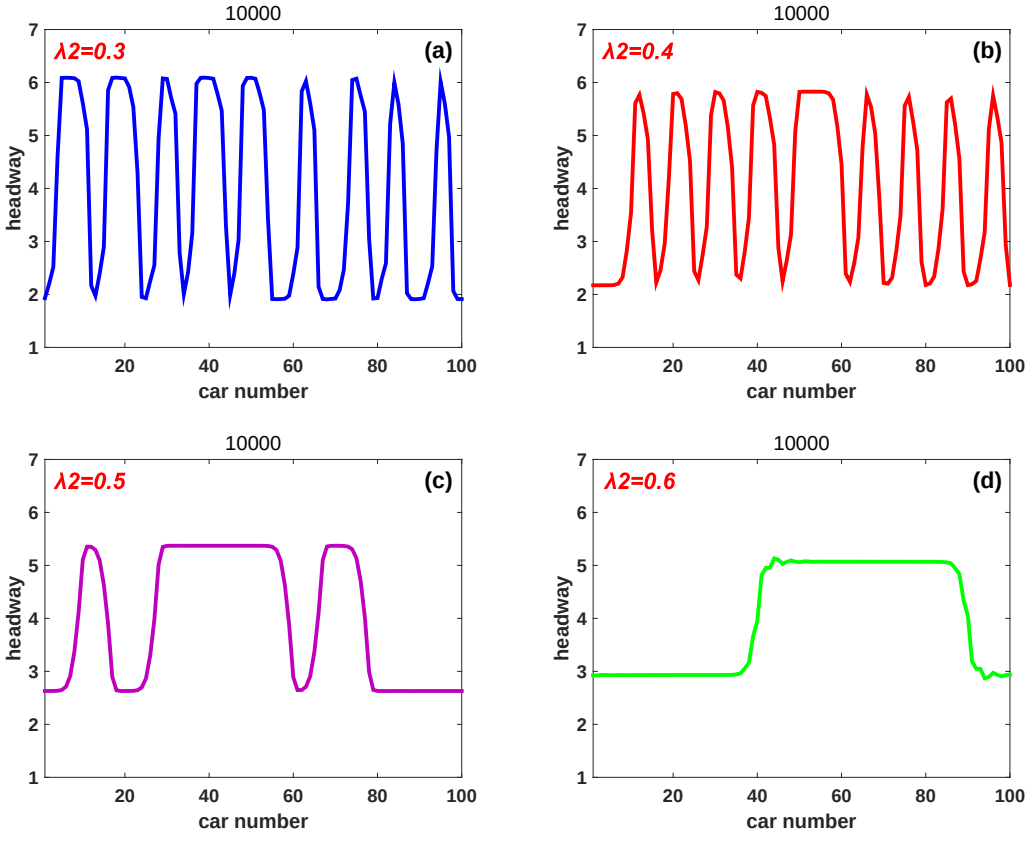

Fig.3. Headway profiles of the density wave at t =10,300 correspond to Fig.2, respectively.

Figure 2 shows the space-time evolution of the headway after $t = 10^4$ time steps under the different parameter λ_2. Other parameters are assumed as: $v_{max} = 2.0$, h_c=4.0. It indicates the kink-antikink solutions propagating backwards. In Fig.2, the typical traffic patterns(a)-(d) exhibit the space-time evolution of the headway corresponding to the cases of λ_2=0.3, 0.4, 0.5, 0.6 respectively. Pattern (a) with λ_1=0.2 and γ=0.1, the result shows that the traffic flow is very chaotic and unstable. When a small disturbance is added into the uniform traffic flow, the propagating backward stop-and-go traffic jam appears which is quite similar to the mKdV solution. From pattern(b) to pattern(d) in Fig.2, the extended traffic flow model congestion situation has a large improvement. In a word, the traffic flow will be smoother while the γ is smaller. Finally the traffic congestion will be eased.

Figure 3 shows the headway profiles and density waves for different the two velocity difference model parameter λ_2 at t = 10300 corresponding to panels in Fig.2, respectively. Then we get the similar outputs to Fig.2. Gradually, as increasing the parameter λ_2, the amplitude of the kink-antikink solition is weakening. Therefore, the traffic flow model has gradually become stable.

Figure 4 shows the space-time evolution of the headway after $t = 10^4$ time steps under the different parameter γ. Other parameters are the same. A battery of simulations are carried out under the periodic conditions for the extended car-following model with different parameters γ. It can exhibit the kink-antikink solutions propagating backwards. From pattern (a) with λ_1=0.2, λ_2=052 in Fig.4 and other parameters are unchanged, it is clearly shown that the traffic is very chaotic and unstable. When a small disturbance is added into the uniform traffic flow, the propagating backward stop-and-go traffic jam appears which is very similar to the mKdV solution. From pattern(b) to pattern(d), the extended traffic flow model congestion situation has a larger improvement. Especially, when the parameter γ is the minimal, the heavy traffic flow becomes the most stable. In general terms, the scales of headway decrease accordingly with the increase of γ, which implies that the traffic flow will be smoother with each passing day.

Figure 5 exhibits the headway profiles and density waves for different λ_2 at t = 10300 corresponding to panels in Fig.4, respectively. And then we obtain the similar outputs to Fig.4. In a word, it is obviously that the traffic flow model is becoming stable gradually as increasing the parameter λ_2.

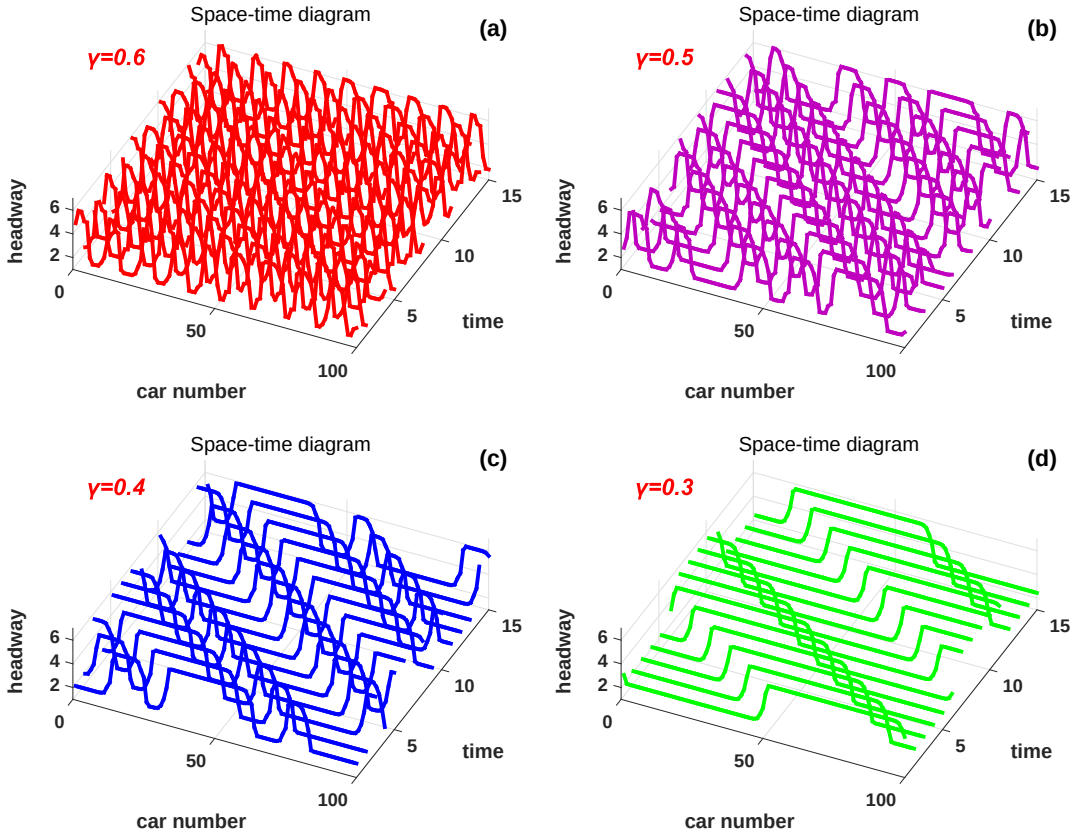

Fig.4. Space – time evolution of the headway after t=10,000 with the different γ-values.

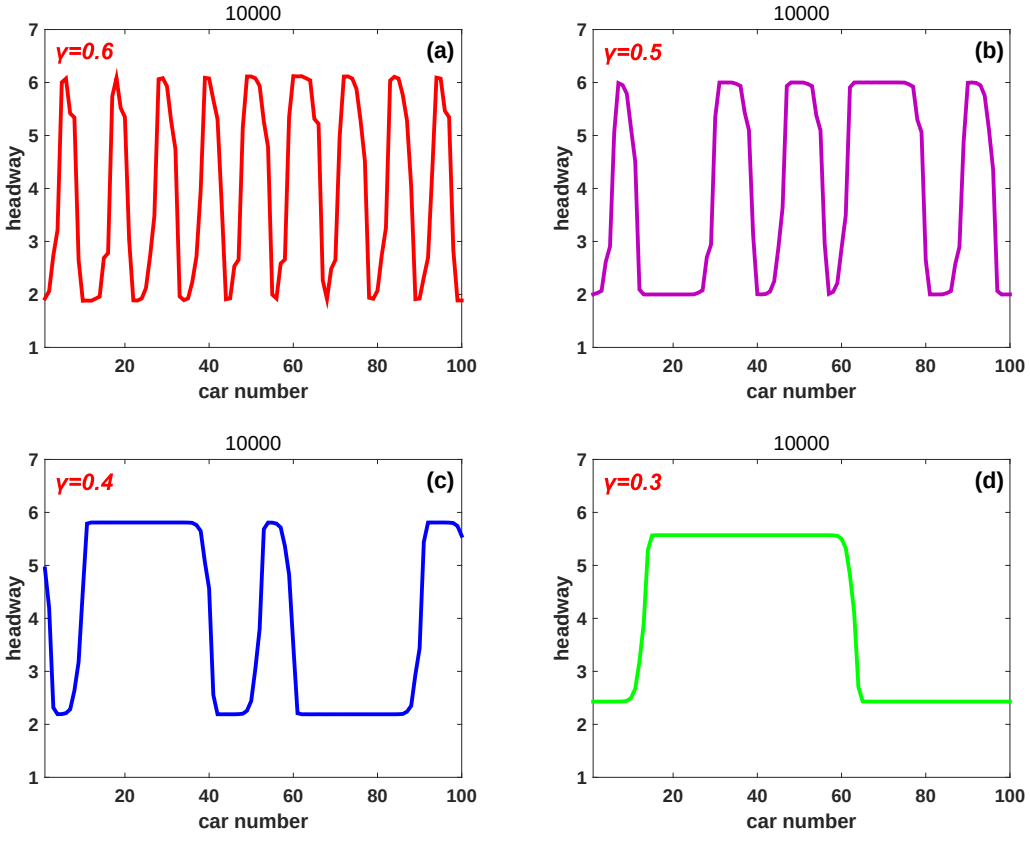

Fig.5. Headway profiles of the density wave at t =10,300 correspond to Fig.4, respectively.

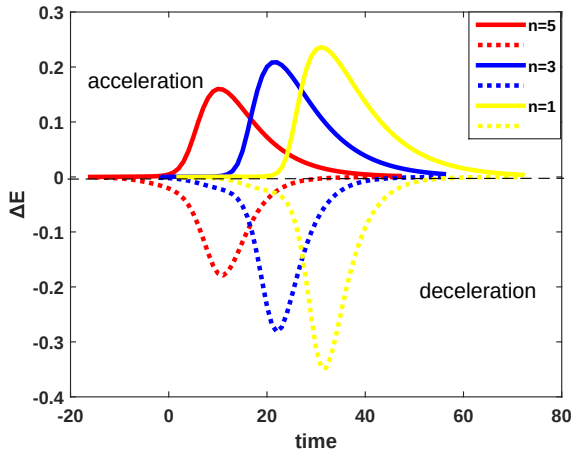

Fig.6 Profile of energy consumption of vehicle according to different values of parameter n.

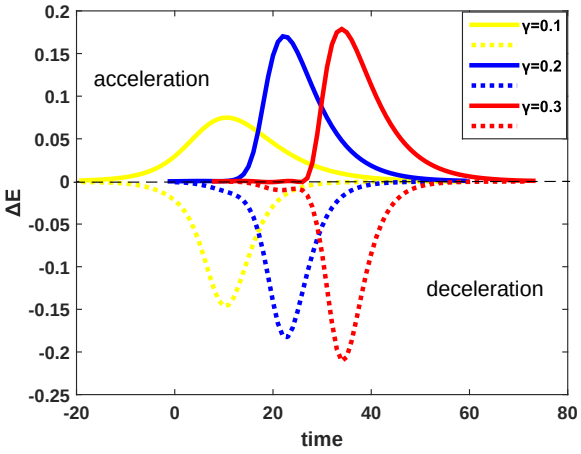

Fig.7 Profile of energy consumption of vehicle according to different values of parameter γ.

Figure 6 shows the distribution of energy consumption for the models with different parameter n. The red curve denotes the model with n=5. The area of loop is the tiniest, so it is the most steady. The blue curve indicates the model with n=3 and the yellow curve denotes the model with n=1, respectively.

Figure 7 shows the distribution of energy consumption for the models with different parameter γ. The red curve denotes the model with γ=0.3. The area of loop is the largest, so it is the most unstable. The blue curve indicates the model with γ=0.2 and the yellow curve denotes the model with γ=0.1, respectively.

From the Fig.6 and Fig.7, we can see two regions with ΔE<0 and ΔE>0. It indicates the acceleration process and deceleration process. On the one hand ΔE<0 denotes the energy consumption in the deceleration process of a vehicle, on the other hand ΔE>0 describes the energy consumption of vehicle during acceleration. It is clear that the area of the acceleration

process and the deceleration process are not symmetrical from the diagram. The area of the deceleration process is larger than the area of the acceleration process. The results show that the energy consumption of the deceleration process is more than the acceleration process. From the diagrams, the energy consumption has decreased with the increase of n and has decreased with the decrease of γ.

6. Conclusion

The above analysis proved that the extended control item did improvement to the stability of traffic flow. In our paper, an improved car-following model of traffic flow basing on the TVDM is put forward to describe traffic phenomena. It takes the influence of the average speed effect of the vehicles and driver's memory into account on traffic flow. By the linear stability analysis, we acquire the neutral stability line and the critical point by the linear stability analysis. And the TDGL equation has been derived to describe the traffic behavior near the critical point by using the reductive perturbation method. In addition, the mKdV equation has been inferred and shown the relationship between the TDGL and the mKdV equations. From the perspective of energy consumption, the stability of traffic flow has been analyzed. Finally, the results of the analysis are in good agreement with the numerical simulation results.

Acknowledgements

Supported by the National Natural Science Foundation of China (Grant No. 61773290), the Scientific Research Fund of Zhejiang Provincial, China (Grant Nos. LY15A020007, LY15E080013), and the K.C. Wong Magna Fund in Ningbo University, China.

References

[1] T.Q. Tang, K.W. Xu, S.C. Yang and H.Y. Shang, Mod. Phys. Lett. B **30**, (2016) 1650084.

[2] Z.P. Li, X. Xu, S.Z. Xu and Y.Q. Qian, Commun. Nonlinear Sci. **42**, (2017) 132-145.

[3] J. Chen, L. Lin and R. Jiang, Phys. A **465**, (2017) 347-357.

[4] L.T. Guo, X.M. Zhao, S.W. Yu, X.H. Li and Z.K. Shi, Phys. A **471**, (2017) 436-444.

[5] T.Q. Tang, Y.P. Wang, X.B. Yang and Y.H. Wu, Nonlinear Dyn. **70**, (2012) 1397-1405.

[6] R. Jiang, M.B. Hu, H.M. Zhang, Z.Y. Gao, B. Jia and Q.S. Wu, Transport Res. B: Meth. **80**, (2015) 338-354.

[7] G.H. Peng, W.Z. Lu, H.D. He and Z.H. Gu, Mod. Phys. Lett. B **31**, (2017) 1750103.

[8] F.X. Liu, R.J. Cheng, H.X. Ge and S.M. Lo, Nonlinear Dyn. **85**, (2016) 1469-1478.

[9] Z.P. Li, W.Z. Li, S.Z. Xu, Y.Q. Qian and J. Sun, Phys. A **436**, (2015) 729-738.

[10] G.H. Peng, Mod. Phys. Lett. B **29**, (2015) 1550174.

[11] Y. Xue, Y. Guo, Y. Shi, L.Z. Lv and H.D. He, Nonlinear Dyn. **88**, (2017) 145-156.

[12] Z.P. Li and Y.C. Liu, Chin. Phys. **15**, (2006) 1570-1576.

[13] S.W. Yu and Z.K. Shi, Nonlinear Dyn. **82**, (2015) 731-740.

[14] T.Q. Tang, Q. Yu, S.C. Yang and C. Ding, Mod. Phys. Lett. B **29**, (2015) 1550157.

[15] T.Q. Tang, Y.H. Wu, L. Caccetta and H.J. Huang, Phys. Lett. A **375**, (2011) 3845 – 3850.

[16] L. Li, F. Wang, R. Jiang, J.M. Hu and Y. Ji, Chin. Phys. B **19**, (2010) 020513.

[17] H.X. Ge, X.P. Meng, J. Ma and S.M. Lo, Phys. Lett. A **377**, (2012) 9-12.

[18] S.W. Yu, X.M. Zhao, Z.G. Xu and Z.K. Shi, Phys. A **461**, (2016) 446-455.

[19] Y. Xue, L.Y. Dong, Y.W. Yuan and S.Q. Dai, Acta Phys. Sin. **51**, (2002) 492-496.

[20] T. Nagatani, Phys. A **264**, (1999) 581-592.

[21] T. Nagatani, Phys. Rev. E **58**, (1998) 4271-4276.

[22] T. Nagatani, Phys. Rev. E **59**, (1999) 4857-4864.

[23] X.Q. Li, K.L. Fang and G.H. Peng, Phys. A **468**, (2017) 315-321.

[24] G.H. Peng, Commun. Theor. Phys. **60**, (2013) 485-490.

[25] Z.P. Li, F.Q. Liu and J. Sun, Chin. Phys. B **20**, (2011) 088901.

[26] R.J. Cheng, H.X. Ge and J.F. Wang, Phys. Lett. A **381**, (2017) 1302-1312.

[27] T. Nagatani, Phys. A **261**, (1998) 599-607.

[28] J. Zhou and Z.K. Shi, Nonlinear Dyn. **81**, (2015) 1247-1262.

[29] G.H. Peng, F.Y. Nie and S.H. Wang, Commun. Theor. Phys. **60**, (2013) 707-713.

[30] M. Bando, K. Haseba, A. Nakayama, A. Shibata and Y. Sugiyama, Phys. Rev. E **51**, (1995) 1035-1042.

[31] D. Helbing and B. Tilch, Phys. Rev. E **58**, (1998) 133-138.

[32] R. Jiang, Q.S. Wu and Z.J. Zhu, Phys. Rev. E **64**, (2001) 017101.

[33] R. Jiang and Q.S. Wu, Chin. Phys. B **375**, (2007) 297-306.

[34] H.X. Ge, R.J. Cheng and Z.P. Li, Phys. A **387**, (2008) 5239-5245.

[35] G.H. Peng, F.Y. Nie, B.F. Cao and C.Q. Liu, Nonlinear Dyn. **67**, (2012) 1811-1815.

[36] D.W. Liu, Z.K. Shi and W.H. Ai, Commun. Nonlinear Sci. **47**, (2017) 139-150.

[37] Y. Xue, Chin. Phys. B **11**, (2002) 1128-1134.

[38] J.Y. Liang, W.Z. Ten and Y. Xue, Acta Phys. Sin. **62**, (2013) 024706.